Winter intrusions of Atlantic Water in Kongsfjorden: oceanic preconditioning and atmospheric triggering

Francesco De Rovere[1,2], Davide Zanchettin[1], Angelo Rubino[1], Leonardo Langone[2], Francesco Calogiuri[3], Paolo Ruggieri[3], Angelo Lupi[2], Jacopo Chiggiato[4]

[1] Department of Environmental Sciences, Informatics and Statistics, Ca' Foscari University of Venice, Venezia, Italy

[2] Consiglio Nazionale delle Ricerche, Istituto di Scienze Polari (CNR-ISP), Bologna, Italy

[3] Department of Physics and Astronomy, University of Bologna, Bologna, Italy

[4] Consiglio Nazionale delle Ricerche, Istituto di Scienze Marine (CNR-ISMAR), Venezia, Italy

Key points:

- Sudden intrusions of Atlantic Water in Kongsfjorden during winter are triggered by abrupt reversals of local meridional winds
- The geostrophic control is disrupted by the advection of anomalously low salinity waters in the fjord, opening the fjord to AW intrusions
- The 2014 Atlantic Water intrusion was triggered by long-lasting southerly winds, transporting warm surface waters toward the fjord

Plain Language Summary

Kongsfjorden is an Arctic fjord in Svalbard, which is largely influenced by the West Spitsbergen Current (WSC), transporting warm and salty Atlantic Water (AW) into the Arctic. In the fjord, occasional winter intrusions of AW occur, leading to abrupt warming events. We found that such intrusions are triggered by wind reversals, i.e., energetic winds from the south followed by winds from the north, which uplift AW from the WSC and guide it toward Kongsfjorden. However, AW can enter the fjord only in those winters characterized by a fjord density lower than that of the WSC, which typically follows a large freshwater production through summer Arctic sea-ice melting in the Barents Sea. Hence, the atmosphere initially triggers the AW intrusion, while ocean conditions defining each winter are a key preconditioning factor opening the fjord to the intrusion. A second mechanism is observed only in 2014: winds from the south blew continuously for two months and transported surface AW from the WSC to the fjord, eventually forcing AW to intrude near the surface, on top of denser local waters.

Abstract

Kongsfjorden is an Arctic fjord in Svalbard, which is largely influenced by the West Spitsbergen Current (WSC), transporting warm and salty Atlantic Water (AW) into the Arctic. The geostrophic control typically prevents AW from entering the fjord in winter, whereas energetic wind events develop the Spitsbergen Trough Current (STC), ultimately flooding fjords facing the West Spitsbergen Shelf with AW. However, an exhaustive understanding of the interplay between these two opposite mechanisms and a clear knowledge of conditions leading to AW winter intrusions are still lacking. In this study, observational and reanalysis data show that wind *reversal* events trigger AW intrusions, while the ocean density is a key preconditioning factor limiting the occurrence of AW intrusions to specific winters only. Wind *reversals* are strong southerly wind events linked to the setup of a high pressure anomaly over the Barents Sea, followed by a circulation reversal with northerly winds. Winters with AW intrusions feature fresher and less dense fjord waters compared to AW, resulting in the breakdown of the geostrophic control mechanism at the fjord mouth, which opens the fjord to waters advected from the WSC by wind *reversals*. The low salinity signal is consistent with a large freshwater production through summer Arctic sea-ice melting in the Barents Sea. Another mechanism is observed only in winter 2014: southern winds blew continuously for two months and transported surface AW from the WSC to the fjord, eventually forcing AW to intrude near the surface, on top of denser local waters.

1. Introduction

The Arctic is acknowledged as a “climatic hotspot” by the scientific community (Meredith et al., 2019). Arctic surface temperatures are increasing at a higher rate compared to the global average since the 1960s, a process named *Arctic amplification* (Chylek et al., 2009; Serreze & Barry, 2011; Richter-Menge and Druckenmiller, 2020), sustaining the loss of Arctic sea-ice volume (Carmack et al., 2015; Comiso, 2012) and the *ice-albedo feedback* (Curry et al., 1995). The Eurasian Arctic is subjected to *Atlantification*, i.e., the propagation of the Atlantic domain toward the Arctic (Lind et al., 2018; Polyakov et al., 2017). The stability of the water column, featuring fresh and cold Arctic Water (ArW) on top and warmer and saltier Atlantic Water (AW) at intermediate/deep layers is being eroded by an enhanced upward flux of heat and salt. Principal consequences are sea-ice melting, warming of the lower atmosphere, a change in air-ocean interactions and in the ecosystem structure (Ingvaldsen et al., 2021). The Svalbard archipelago is set in the Eurasian Arctic and surrounds the eastern side of the Fram Strait, the main gateway of AW to the central Arctic basin. The largest island, i.e., Spitsbergen, presents different broad fjords on its western side: Kongsfjorden, Isfjorden, Bellsund and Hornsund. The hydrography and climate of these fjords are largely influenced by the two main currents of the region: the West Spitsbergen Current (WSC) and the Spitsbergen Polar Current (SPC) (Helland-Hansen & Nansen, 1909). The barotropic and topographically steered WSC transports AW northward along the continental slope. The WSC is characterized by a strong seasonality, with the largest AW transport in late autumn and early winter (Beszczynska-Möller et al., 2012b; Walczowski & Piechura, 2011). WSC properties and structure undergo large interannual variability linked to the general oceanic and atmospheric circulation pattern over the North Atlantic (Chatterjee et al., 2018; Muilwijk et al., 2018; Raj et al., 2018; Wang et al., 2020). The SPC flows northward on the West Spitsbergen Shelf (WSS), parallelly to the WSC, and is identified by cross-shelf sloping isopycnals, revealing its geostrophic nature (Svendsen et al., 2002). It carries ArW and sea-ice from Storfjorden and the Barents Sea, and travels on the shallowest layers close to the West Spitsbergen coast. Figure 1 illustrates a map of Spitsbergen and its fjords, along with main currents flowing in the area.

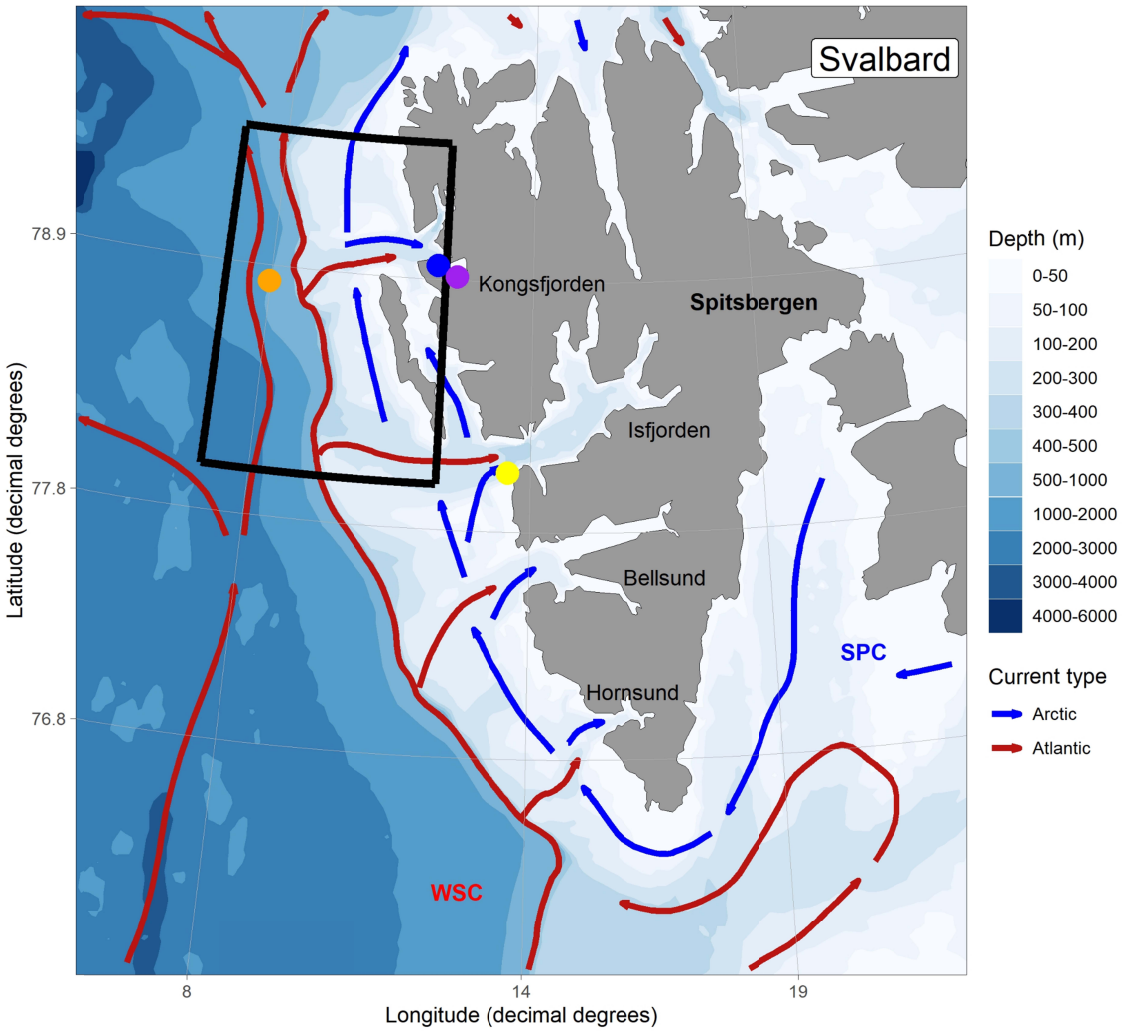

Figure 1: Map of West Spitsbergen with main Arctic (blue) and Atlantic (red) water currents. The four coloured points represent the location of the 4 moorings whose observations are used in this study: MDI (purple), KF (blue), I1 (yellow) and F3 (orange). The black box indicates the area A1, where ERA5 atmospheric wind data are evaluated. The color scale illustrates the bathymetry. This figure has been generated through the PlotSvalbard R package (Vihtakari, 2020).

Kongsfjorden (Hop and Wiencke, 2019) is the northernmost broad fjord in West Spitsbergen, and is connected with WSC waters through a deep trough, Kongsfjordrenna. In the fjord, occasional winter intrusions of AW occur, leading to large positive temperature and salinity anomalies. AW in Kongsfjorden is defined by Tverberg et al. (2019) as water with $T > 3°C$ and salinities larger than 34.9. ArW instead is defined as Local Water (LW) and indicates those waters with $T < 1°C$. Variable dilutions between LW and AW take the form of

Intermediate Water and Transformed Atlantic Water. Different mechanisms have been proposed to explain AW intrusions in Kongsfjorden. A geostrophic control mechanism prevents shelf waters from entering the fjord, especially during the winter season (Cottier et al., 2005; Klinck et al., 1981; Svendsen et al., 2002). The degree of control is determined by the strength of the SPC, depending primarily on the shelf-fjord density gradient. When the coastal current faces larger densities on the right, i.e., when the density in the fjord is larger than that on the shelf, its strength will increase with increasing depths. This condition is typical of winter months when fjord heat loss to the atmosphere and sea-ice production increase density in the deep fjord basin. As a result, AW advected near the bottom through Kongsfjordrenna will join this current at the fjord mouth, making a detour northward. On the opposite, when shelf waters are denser than fjord waters, typically in summer months, during which large amounts of freshwaters are released from local glaciers, the speed of the coastal current will decrease with depth. The geostrophic control mechanism breaks down and WSC waters are free to enter the fjord at intermediate and large depths, while the coastal current is confined in the upper layers. Density variations on the shelf develop horizontal pressure gradients between the fjord and the shelf driving baroclinic currents (Klinck et al., 1981; Stigebrandt et al., 1981; Svendsen et al., 1980). Such variations are generated by wind convergence and divergence near the coast, causing downwelling and upwelling, or by advection of horizontal density gradients along the coast. Strong southerly winds and a negative wind curl over the WSS can stack up less dense surface waters along the coast. Once the wind ceases, the water column on the shelf returns to a normal stratification state and the fjord adjusts to it with an outflow near the surface and an inflow near the bottom. Episodes of this “intermediary circulation” have been observed also in Greenland fjords (Jackson et al., 2014; Straneo et al.; 2010). Wind events on the shelf can also lead to geostrophic advection of WSC waters into West Spitsbergen fjords through the development of the Spitsbergen Through Current (STC) (Nilsen et al., 2016). Water convergence near the coast enhances the positive gradient in the surface tilt over the shelf break. As a result, both the WSC and the SPC are strengthened (Teigen et al., 2010), and the WSC is moved on shallower isobaths on the WSS, generating the topographically guided STC. Once the wind turns northerly, upwelling of the STC starts on the shelf. Nilsen et al. (2016) and Cottier et al. (2007) suggest that the resulting offshore surface current on the shelf opposes the SPC and can break down the geostrophic control mechanism, allowing the STC to intrude in West Spitsbergen fjords. The strong southerly wind events described by Nilsen et al. (2016) are the so-called winter cyclones. Strong blocking conditions developing over Scandinavia and Europe stretch the Atlantic storm track over the Greenland Sea to the Arctic, including Svalbard (Häkkinen et al., 2011; Rogers et al., 2005; Ruggieri et al., 2020), generating southerly winds over the eastern Fram Strait and the arrival of warm

and humid air masses over Svalbard. Other effective means of shelf-fjord exchanges are instabilities at the WSC-SPC front, developing topographic waves (Nilsen et al., 2006; Teigen et al., 2010, 2011). Stable topographic waves are generated by wind events at the shelf-edge front and can develop coastally trapped waves traveling along isobaths on the steep southern side of Kongsfjordrenna (Inall et al., 2015).

Atlantification is leaving its footprint on West Spitsbergen fjords by increasing their water temperatures and salinities (Bloshkina et al., 2021; Cottier et al., 2019; De Rovere et al., 2022; Skogseth et al., 2020; Strzelewicz et al., 2022; Tverberg, et al., 2019). After 2006, winters became more Atlantic-like with no sea ice and occasional shallow AW advection (Tverberg et al., 2019). Furthermore, the occurrence of intense winter cyclones passing over Svalbard in winter is increasing (Zahn et al., 2018), potentially boosting winter AW advection on the WSS and adjacent fjords. An increasing heat content in the fjord affects also the stability of ecosystem's structure (Hegseth and Tverberg, 2013; Payne and Roesler, 2019; Vihtakari et al., 2018) and tidewater glaciers (Holmes et al., 2019; Luckman et al., 2015). Henceforth, the dynamics of AW winter intrusions should be interpreted to fully understand ongoing changes in Kongsfjorden and its future evolution, especially under the influence of *Atlantification* and *Arctic amplification*. To the best of our knowledge, a clear examination of AW winter intrusion events in the fjord after the 2006/2007 event is lacking. In addition, there is a need to robustly define common traits, especially the large-scale atmospheric and oceanic settings leading to AW winter intrusions. In particular, the relation and interplay between the two most important mechanisms, i.e., the STC and the geostrophic control mechanism, are not clearly defined. Despite being a very important factor driving dynamics on the WSS, a complete understanding of the SPC's influence on winter water masses variability in Kongsfjorden is still to be defined (Tverberg et al., 2019). The scientific community now has access to *in-situ* continuous measurements acquired over the 2011-2020 decade from several mooring lines in the West Spitsbergen area. Exploiting the availability of such an extensive dataset and high-resolution reanalysis products (ERA5), a deep joint examination of the typical mechanisms leading to AW winter intrusions in Kongsfjorden can now be performed. Oceanographic observations in Kongsfjorden are not just describing current conditions and ongoing changes in the fjord itself, but can be indicators for the other West Spitsbergen fjords as well as for similar shelf-fjord systems in the Arctic.

The aim of this work is to investigate winter (January to March) AW intrusions in Kongsfjorden during the 2011-2020 decade by jointly examining local and large-scale atmospheric and oceanic dynamics, combining *in-situ* and reanalyzed observations. The specific objectives are: to give a concise overview of winter AW intrusions occurred in the

2011-2020 decade in Kongsfjorden and to assess the dynamics of such events, particularly the large-scale atmospheric and oceanic conditions.

This paper is organized as follows: Section 2 provides an overview of the data utilized in this study and the methods for data analysis. Section 3 combines the presentation of the results with a discussion. Section 4 provides a summary and illustrates the main conclusions of this study.

2. Data and Methods

2.1 Data

2.1.1 In-situ data

In-situ oceanic observations in Kongsfjorden are retrieved by two mooring lines: MDI and KF. The former is managed by the Institute of Polar Sciences of the National Research Council of Italy (CNR-ISP). MDI is anchored at approximately 105 m depth in inner Kongsfjorden and has been monitoring temperature and salinity at 85 m since September 2010 (D'Angelo et al., 2018; De Rovere et al., 2022). KF is located in the mid fjord at approximately 260 m depth, and is managed by the University of Tromso (UiT) in collaboration with the Scottish Association for Marine Sciences (SAMS). Two continuous temperature and salinity records are available from 2006 to 2018, except for 2012, at the near surface (circa 30 m depth) and the near-bottom (circa 230 m depth). KF has also been supplied with several thermistors at different depths, allowing for the representation of temperature along the water column. Furthermore, KF is equipped with two ADCPs providing current data. Ocean current observations are averaged in the vicinity of temperature and salinity sensors, at 20-30 m (near-surface) and 200-210 m (near-bottom) depth, and their tidal frequencies removed. The University Centre in Svalbard (UNIS) is maintaining the I1 mooring, situated in the southern end of Isfjorden's mouth. Temperature and salinity observations at 190 m depth are assessed to depict conditions on the shelf adjacent to Isfjorden. The Alfred Wegener Institute, Helmholtz Center for Polar and Marine Research (AWI) ran a monitoring program composed of a mooring array positioned in the Fram Strait from late 1990s to 2016 (Beszczynska-Möller et al., 2012b). We selected one mooring, i.e, F3, positioned at the shelf break and whose temperature and salinity data collected at 250 m depth describe the properties of the WSC. *In-situ* local atmospheric observations in Kongsfjorden as air temperature, relative humidity and winds, are retrieved from the Climate Change Tower (CCT) located in the village of Ny-Alesund, on the southern side of the fjord.

2.1.2 Reanalysis datasets

Winds at 10 m height and geopotential height fields at 850 hPa over the Arctic and Fram Strait regions are utilized to describe large-scale atmospheric conditions. Data are retrieved from ERA5 reanalyses. Wind and wind curl data are averaged over an area representative of the WSS adjacent to Kongsfjorden (A1, black rectangle reported in Figure 1; 7-12 °E, 78-79.5 °N). We also use salinity fields at 50 m depth from the CMEMS Arctic Ocean Physics Reanalysis to define the large scale oceanic conditions in Svalbard and the Barents Sea. Data regarding the main northern Atlantic hemispheric teleconnection patterns are retrieved from the NOAA Climate Prediction Center and are: the North Atlantic Oscillation, the Arctic

Oscillation, the East Atlantic Pattern, the East Atlantic/Western Russia pattern, Scandinavia Pattern.

2.2 Methods

All data were averaged at a daily frequency, except for climate indices. We choose the *onset date* (t = 0) of AW intrusion events by selecting the time of a large and sudden increase in temperature and salinity in Kongsfjorden *in-situ* oceanic observations from MDI and KF (see Section 3.1 and Figure 2 for more details). We determine the peculiar atmospheric conditions characterizing AW intrusion events through a Superposed Epoch Analysis (SEA) (Chree, 1912; Chree, 1913; Singh, 2006). This technique allows to detect common features shared by target events against background noise. We select the onset dates (t = 0) of the AW intrusion and we average conditions over the previous week ($-7 <= t <= -1$) and the following week ($0 <= t <= 6$). The two weekly means calculated for each event are then averaged into two single averages in the case of punctual time series, or two maps as in the case of two-dimensional atmospheric fields.

3. Results and discussion

3.1 Definition of Atlantic Water intrusion events

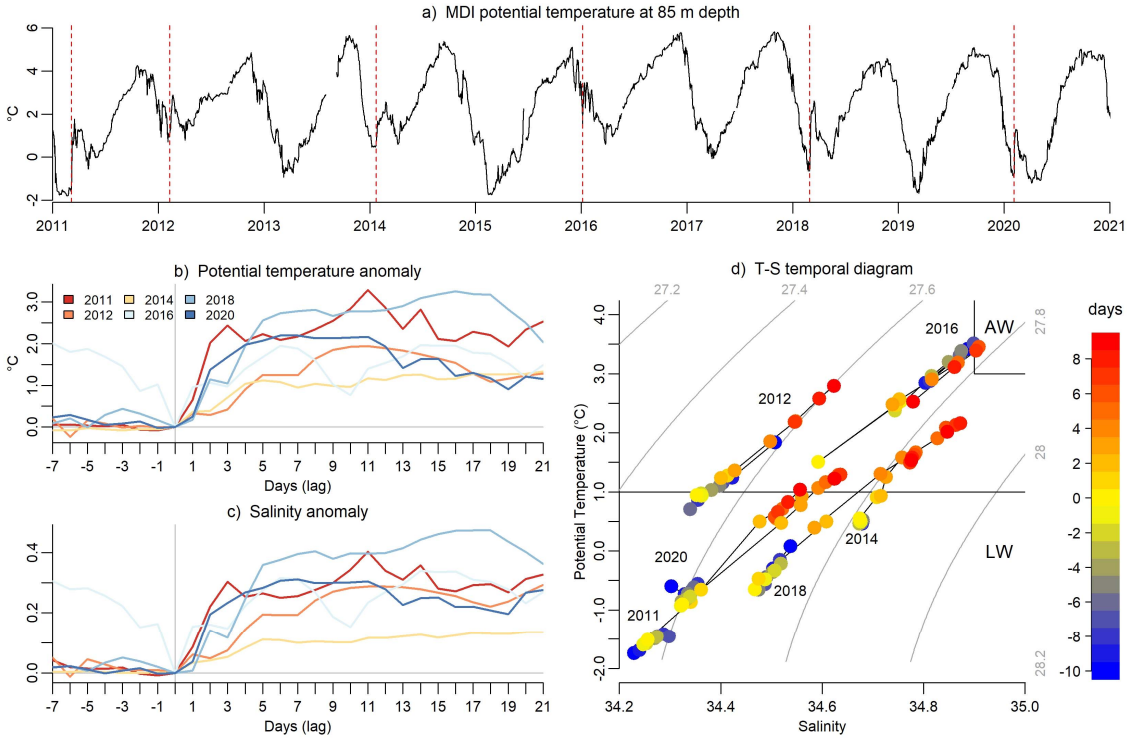

Figure 2: Definition of AW intrusion events as from MDI observations. a) Daily averaged temperature at 85 m depth with dashed red lines indicating the selected onset of AW intrusion events. b) Potential temperature and c) salinity daily anomaly series at 85 m depth around the AW intrusions. Anomalies are calculated by subtracting the temperature and salinity value of the onset day from the two series, respectively. The two series have been lagged so that the onset of each event corresponds to lag=0. d) T-S diagrams representing 85 m depth observations acquired from day -10 to day +9 for each event.

Figure 2a reports the ocean temperature observed by MDI at 85 m depth in inner Kongsfjorden, from 2011 to late 2020. We identified 6 winter AW intrusion events occurring in 2011, 2012, 2014, 2016, 2018 and 2020. The events feature large and sudden increases in water temperature and salinity, as reported in Figure 2b-c. Onset dates (see section 2.2) are labeled by vertical dashed red lines in Figure 2a and the zero lag vertical line in Figure 2b-c, and are the following: 2011-03-07, 2012-02-11, 2014-02-24, 2016-01-06, 2018-03-01, 2020-02-04. The largest temperature change takes place within the first 5 days from the *onset*. In this time range, the greatest temperature growth occurred in 2018 (2.51 °C), while the lowest in 2014 (1.1 °C). Figure 2d reports a T-S diagram showing the temperature and salinity evolution in the neighborhood of each event. LW is present in inner Kongsfjorden in

253 the days before the event are then replaced by variable dilutions with AW. This represents a
254 clear signal of an AW intrusion event from the WSC to Kongsfjorden. The winter 2016 event
255 is peculiar since it is not characterized by a single intrusion event but by several short-lived
256 events.
257
258 3.2.1 Mechanism for upwelling events
259 AW intrusions occurred in 2011, 2012, 2016, 2018 and 2020 shared common dynamics,
260 where warmer temperatures propagate from the fjord's bottom toward the surface, in a few
261 days. Winter 2018 is reported in Figure 3 as an emblematic example of these "upwelling"
262 events, while the others are reported in supplementary Figures S1 to S4. In these figures,
263 besides MDI data, we make use of the oceanographic observations from mooring KF, as
264 well as *in-situ* and reanalysis atmospheric data, to examine the local oceanic and
265 atmospheric variability.
266

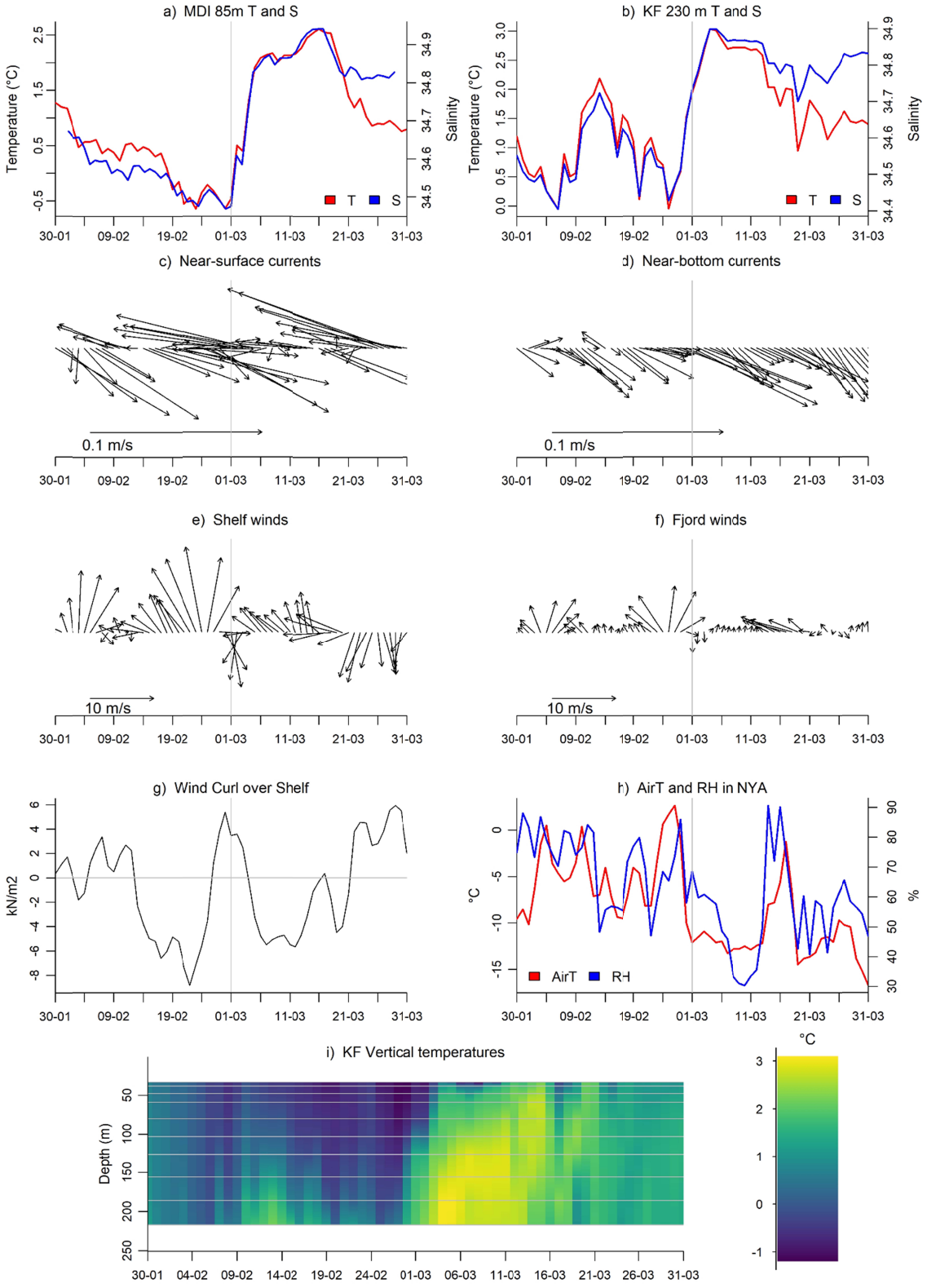

Figure 3: Winter 2018 as representative of upwelling events: temperature and salinity at MDI (a) and KF (b); near-surface (c) and near-bottom (d) currents from KF; average winds (e) and wind stress curl (g) over A1 from ERA5; fjord winds (f) and meteorological conditions (h)

from the CCT; (i) KF temperature profile with gray horizontal lines identifying sensors' depths.

The warming signal at KF (Figure 3b) precedes MDI (Figure 3a) by approximately 3-4 days in each intrusion event by upwelling. Another weaker warm water intrusion occurred near mid-February 2018 near the bottom, which does not propagate toward the surface, as it is detected only at 230 m depth and not at 85 m. The AW intrusion is accompanied by large outflowing current velocities near the surface (Figure 3c) and large inflowing current velocities at depth (Figure 3d), both along the main fjord axis. Instead, days preceding the intrusion's *onset* feature inflowing currents near the surface and very low velocities near the bottom. Shelf winds are primarily southerly in the week before the *onset* and then turn northerly in the week after the *onset*. We name these atmospheric events as *reversals.* Winds in the fjord reflect the main evolution observed on the shelf (Figure 3f). Southerlies bring very warm and humid air, rising air temperatures in Kongsfjorden even above zero for some days, then replaced by cold and dry air brought by northerlies after the *onset date* (Figure 3h). The average wind curl is largely negative before the *onset*, turning to positive when KF temperature increases. This atmospheric evolution over the West Spitsbergen area appears to be the key common mechanism triggering upwelling warming events in Kongsfjorden (see also Figure S1 to S4). This dynamic is consistent with the development of the STC on the WSS (Nilsen et al., 2016) and the intermediary circulation between Kongsfjorden and Kongsfjordrenna (Stigebrandt et al., 1981). Southerly winds and the negative wind curl force surface waters to stack up along the West Spitsbergen coast. The resulting increase in the cross-shelf sea surface tilt forces the WSC on shallower isobaths on the shelf, developing the STC. Once southerly winds cease, the sea-surface tilt relaxes and surface waters tend to flow offshore, compensated by an inflow from the shelf break on the lower levels. AW now can flow at the deepest levels on the shelf toward the fjord. Northerly winds further drive surface waters off Kongsfjorden, which are compensated by the inflow of AW from the STC near the bottom. AW is uplifted by upwelling and reaches the near surface.

3.2.2 Atmospheric triggering: "reversal" events

This section examines the occurrence of wind *reversal* events and the associated large-scale atmospheric patterns. We define wind *reversals* as those events featuring strongly southerly winds ($V > 3$ m/s) blowing on the WSS (area A1) in the week before and northerly ($V < 0$ m/s) in the week after the *onset* of AW intrusion events. The occurrence of wind *reversal* events in the 2011-2020 decade, irrespective of their association with an AW

307 intrusion event, as well as the associated large-scale geopotential and wind stress curl
308 patterns are examined in Figure 4 through ERA5 observations.
309

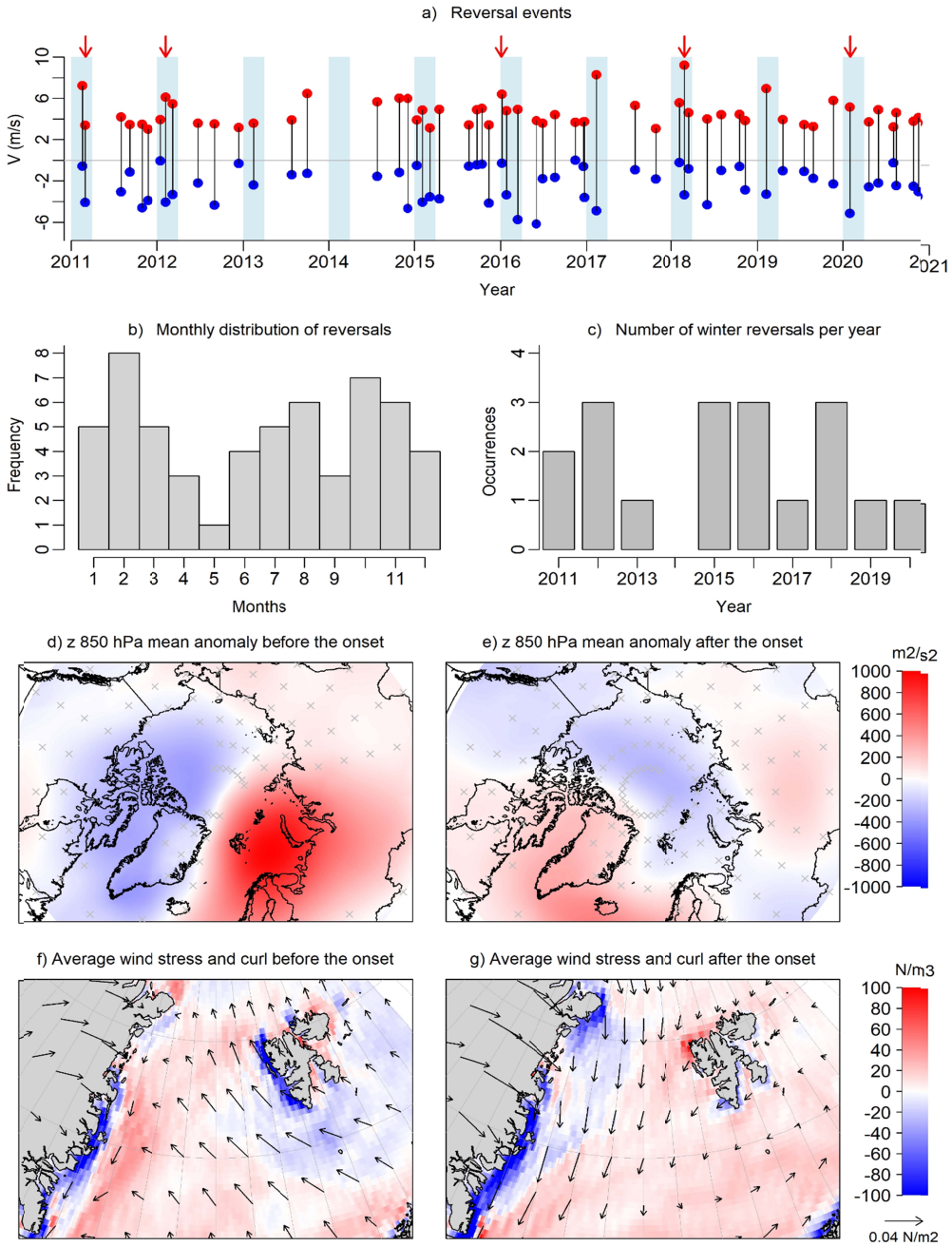

310

311 Figure 4: (a) Average V in the week before (red points) and after (blue points) the *onset* of
312 *reversals*. Blue areas indicate winter months (Jan-Mar). Monthly (b) and yearly (c) frequency
313 of *reversals* during the 2011-2020 decade. Average geopotential anomalies at 850 hPa (d,
314 e), wind stress and wind stress curl (f, g) before and after the onset of *reversals* occurred in
315 the 2011-2020 decade. Geopotential anomalies are calculated considering the 2011-2020

316 time period as climatology. In Figure 4d-e, areas marked with gray crosses are non-
317 significant anomalies (see Appendix A for a complete description of the significance
318 analysis).
319
320 *Reversal* occur throughout the year and are not confined to the winter season, as reported in
321 Figure 4a-b, with two local maxima in February and October. *Reversals* occurred almost in
322 every winter of the decade, up to three events per season (Figure 4c), for a total of 18 winter
323 events. We further examine *reversal*'s characteristics using this larger pool instead of only
324 the five upwelling events to increase the robustness and significance of our results.
325 Atmospheric conditions before and after the onset of *reversal* events reflect two strongly
326 different large-scale/synoptic circulations. Strong southerly wind events in the week before
327 the onset are generated by the setup of a high pressure anomaly centered over the Barents
328 Sea and a low pressure anomaly over north-eastern Canada and Greenland (Figure 4d).
329 This geopotential dipole sets up strong geostrophic winds blowing from the south over the
330 Fram Strait, moving waters toward the physical barrier represented by the West Spitsbergen
331 coast (Figure 4f). In addition, wind stress curl indicates upwelling in the central Fram Strait
332 and strong downwelling on the WSS, this being driven by the slower winds interacting with
333 the terrain over the Svalbard archipelago. The situation changes suddenly in a few days,
334 from daily southerlies of 10 m/s to northerlies of 6-7 m/s. The restoration of a low pressure
335 anomaly over the north pole (Figure 4e), the Svalbard archipelago and the northern Barents
336 Sea triggers northerly winds initiating upwelling on the WSS (Figure 4g), especially on the
337 northern WSS. Note that these negative geopotential anomalies are not significantly different
338 from typical pressure conditions characterizing winter months. The link of these *reversals*
339 with the general atmospheric circulation is further examined through a correlation analysis
340 between the number of winter reversal events per year and the winter average of several
341 teleconnection indices (see Section 2.1.2). The only significant (*p-value*=0.01) correlation (-
342 0.4) is found with the Arctic Oscillation (AO). A negative phase of the AO is associated with a
343 weaker jet stream in the northern hemisphere, characterized by large meanders propagating
344 high pressure anomalies as north as the Barents Sea and Fram Strait and negative pressure
345 anomalies toward the mid-latitudes. A negative AO phase can thus set up a pressure
346 anomaly field at high latitudes characterized by large zonal gradients, a feature consistent
347 with the geopotential dipole observed in Figure 5a, hence increasing the probability of large
348 meridional winds over the Fram Strait.
349 In conclusion, *reversals* are common phenomena occurring throughout the decade, and are
350 not associated to just one season and neither to specific years. An important question arises
351 from this observation: why do AW intrusions occur only in some winters and do not follow
352 every *reversal* event? We hypothesize that *reversals* are not the only key aspect initiating

AW intrusions, despite they develop the STC and set off the movement of AW toward Kongsfjorden. Another key factor opens and closes the fjord to AW intrusion in specific winters, and this role is played by the ocean.

3.2.3 Oceanic preconditioning

The ocean opens and closes Kongsfjorden to AW intrusions through the geostrophic control (Klinck et al., 1981; Cottier et al., 2005). Here we will demonstrate that this mechanism contributes to explain the inter-annual variability in AW winter intrusions in Kongsfjorden, and how the SPC and large-scale oceanic conditions play a key role in preconditioning the fjord in winter.

Figure S5 reports the oceanic conditions in Kongsfjorden in the week before and after the onset of all 2011-2020 winter atmospheric *reversals* from observations acquired by KF and MDI. Three clear features stand out. First, not all *reversals* are followed by a large positive temperature change, as in the case of AW intrusion events by upwelling. Second, the five AW intrusion by upwelling show the largest difference in potential density between fjord bottom waters and inflowing waters (Figure S5a-b), a feature consistent with the disruption of the geostrophic control. Third, the five AW intrusion by upwelling are characterized by low density bottom fjord waters in the week before the *onset*. These low density waters result from the presence of low salinity waters (2011, 2012, 2018, 2020 events) or very warm waters (2016 event). The autumn and winter inter-annual variability in potential density, potential temperature and salinity at KF and MDI is examined in Figure 5.

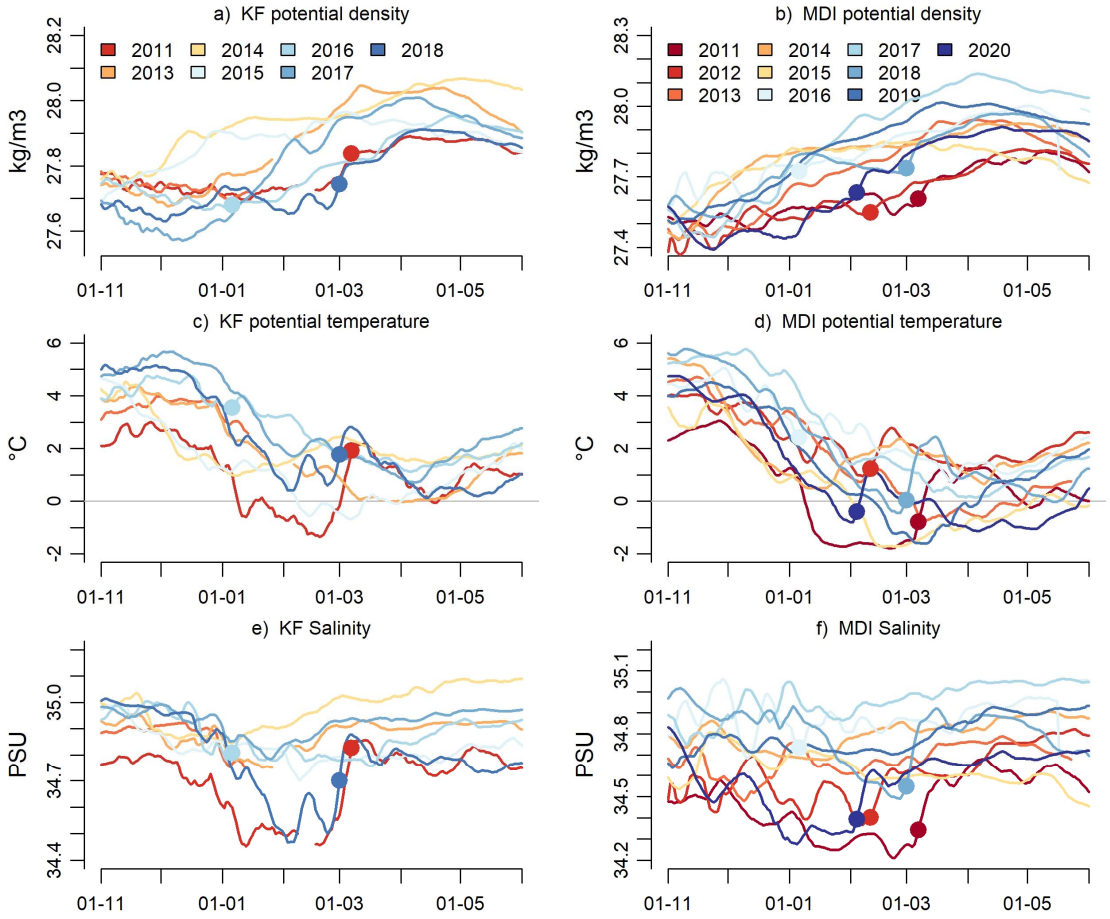

Figure 5: Potential density (a, b), potential temperature (c, d), salinity (e, f) at KF (230 m) and MDI (85 m) between November of the previous year and June of the current year (see legends). Time series are smoothed with a 7-days moving average. Dots indicate the onset of AW intrusion events at MDI, as identified in section 3.1.

Figure 5a-b indicates that low density waters are not confined just within the period preceding the warming, but characterizes the whole winter season of those years with AW intrusions by upwelling in Kongsfjorden: 2011, 2016 and 2018 for KF (Figure 5a); 2011, 2012, 2018 and 2020 for MDI (Figure 5b). Note here that KF has no measurements for winters 2012, 2019 and 2020. The low density is linked to the low salinity signal (Figure 5e) characterizing those winters, apart from 2016. At 230 m depth, salinity in 2011 and 2018 drops right before the beginning of the new year to a local minimum around February. A similar behaviour is observed for MDI (Figure 5f). Here, low salinities characterize January and February of those years with AW intrusion by upwelling, i.e., 2011, 2012, 2018 and 2020, even though here in the inner fjord there is not a clear salinity drop as in the mid fjord. Winter 2016 is a peculiar event as it features several different but frequent AW intrusions

393 events already from the end 2015 (De Rovere et al., 2022), leaving continuous warm and
394 low density conditions in the mid fjord for the whole winter.
395 To better understand how this inter-annual variability in near-bottom density influences the
396 geostrophic control in the winter season, measurements from KF and F3 (WSC at the shelf-
397 slope) are examined in Figure 6.
398
399

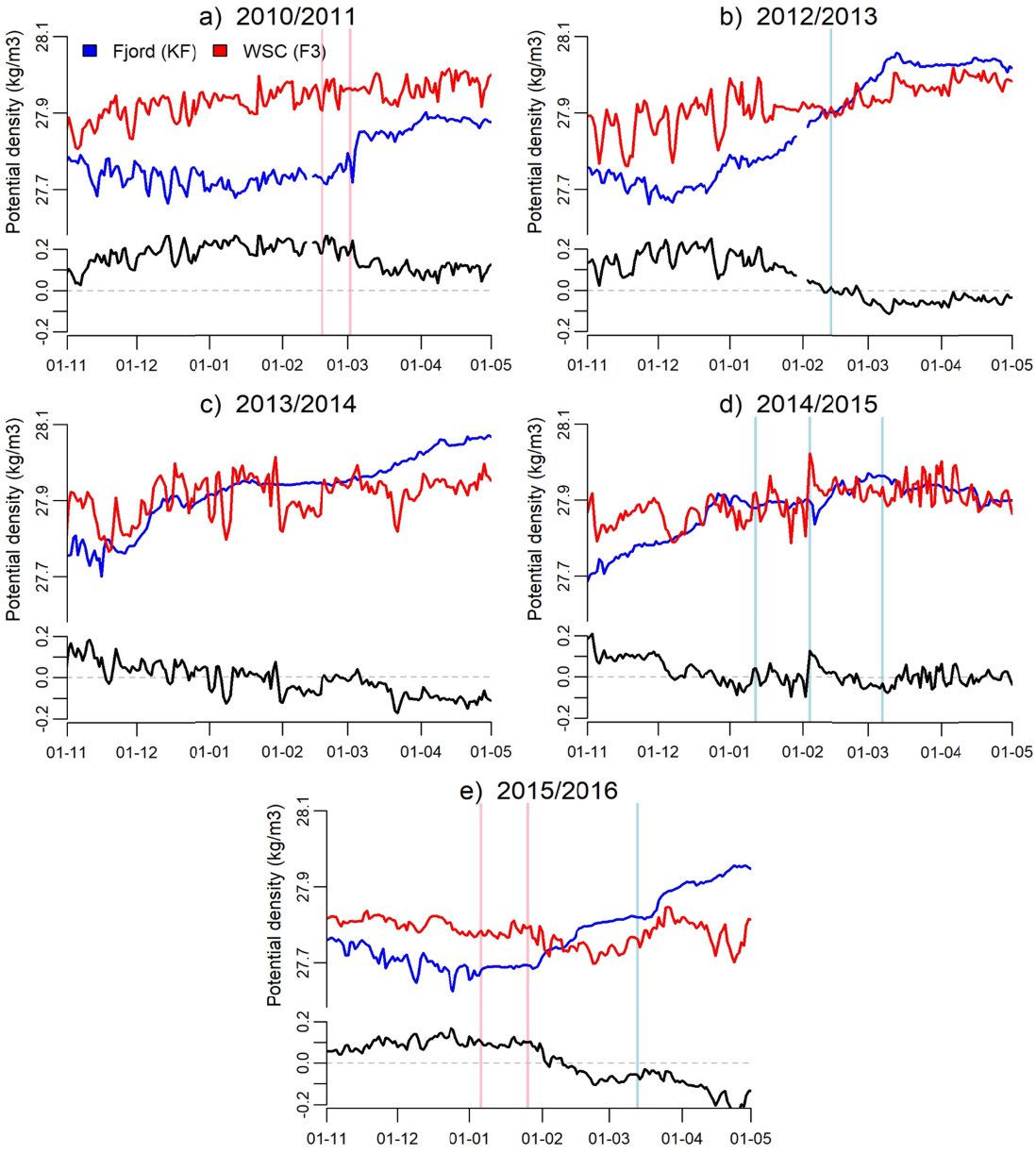

400
401 Figure 6: Potential density at KF (230 m depth, blue lines) and F3 (250 m depth, red lines)
402 between October and May for those years with simultaneous measurements. Dates of
403 *reversals* are represented with vertical blue lines, while vertical red lines identify *reversals*

404 associated with AW intrusions. The lower side of each panel reports the difference between
405 F3 and KF potential densities.
406
407 The potential density of the WSC tends to increase from September to May, except for
408 winter 2016. Fjord density generally grows over the winter season, but the timing of the
409 growth can change from year to year, some in early winter, as 2013, 2014 and 2015, and
410 some other later as 2011 and 2016. This large inter-annual variability in fjord density is a key
411 element affecting the cross-shelf density gradient. *Reversals* occurred in 2011 and 2016
412 found a positive off-shore density gradient (Figure 6a,e), indicating a disrupted geostrophic
413 control, eventually allowing the AW from the STC to flood the fjord. On the contrary,
414 *reversals* occurring in the other winters (Figure 6b,c,d) found a negative off-shore density
415 gradient. This is associated to an active geostrophic control which blocks the AW convoyed
416 by the STC directed toward Kongsfjorden. In this case, northerly winds upwell fjord deep
417 waters.
418 Results indicate that the occurrence of AW winter intrusions in Kongsfjorden is principally
419 linked to winter density conditions, whose inter-annual variability largely depends on the
420 arrival of fresher waters at the fjord near-bottom (2011, 2012, 2018 and 2020). Observations
421 from mooring I1, located on the shelf adjacent to Isfjorden, are investigated to examine the
422 origin of this freshwater signal. Both density and salinity at 160 m depth shows an inter-
423 annual variability consistent with KF and MDI data, featuring lower values during winters
424 characterized by upwelling events (Figure S6). I1 observations also show that winter 2012,
425 which was not recorded by KF, features a low potential density at the beginning of the
426 season, with values comparable to those of 2011 and 2018 winters. Low density waters in
427 years with AW intrusion by upwelling are thus found both in Kongsfjorden and Isfjorden,
428 suggesting a common freshwater source for these two locations. The main freshwater
429 source in winter in the West Spitsbergen area is the SPC, which transport ArW and sea-ice
430 from the Barents Sea through Storfjorden to the WSS. The SPC is thus the primary factor
431 driving the peculiar inter-annual variability in the shelf and fjords' winter density, eventually
432 opening Kongsfjorden to AW winter intrusions once triggered by atmospheric *reversals*. The
433 large-scale salinity conditions in the Eurasian Arctic is examined in Figure 7 to investigate
434 the source of this freshwater signal.
435

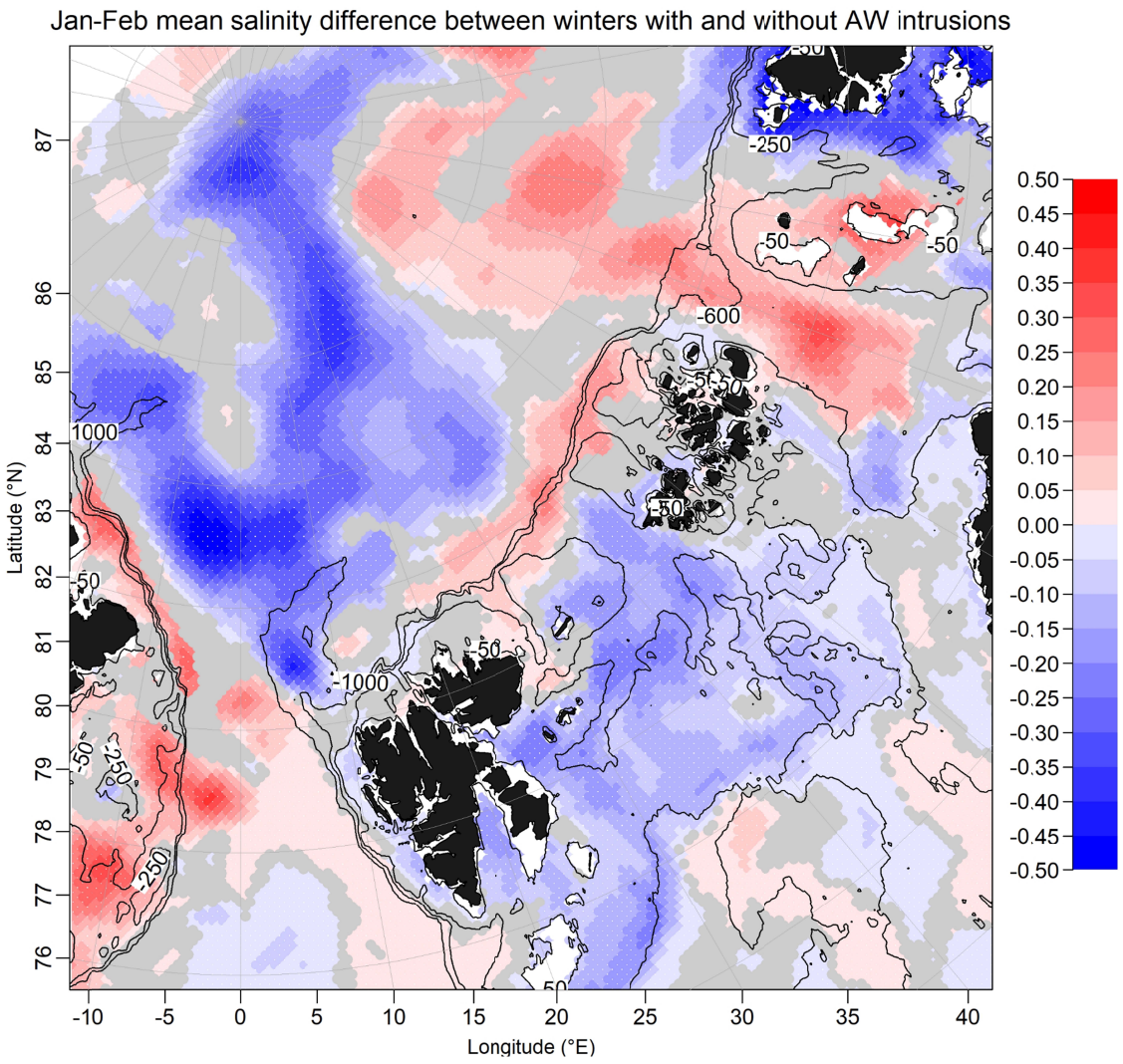

Figure 7: January-February mean salinity difference at 50 m depth between winters with AW intrusions (2011, 2012, 2018, 2020) and winters with no AW intrusion (2013, 2015, 2017, 2019). Blue (red) areas are characterized by lower (larger) salinities during years with AW intrusions in Kongsfjorden. Gray areas identify locations whose two daily salinity pools do not come from two significantly different distributions at the 99% confidence level (see Appendix B). Data are from the CMEMS daily Arctic Ocean Physics Reanalyses.

Significantly lower salinities in the WSS at 50 m depth are seen for those years featuring an AW intrusion by upwelling (2011, 2012, 2018, 2020), compared to the other winters (2013, 2015, 2017, 2019). Besides the WSS, this negative salinity anomaly characterizes Storfjorden and the region south of the Svalbard archipelago, the northern Barents Sea and the central Arctic basin. We hypothesize this winter large scale salinity structure to be consistent with a large export of freshwater from strong sea-ice melting during the previous

summer season. Indeed, the upper ocean in the northern Barents Sea in winter is very sensitive to the freshwater input from melting sea ice in the previous summer season (Lundesgaard et al., 2022). The region at the edge between the Barents Sea and the central Arctic basin, corresponding roughly to the summer sea-ice transition zone, features a positive salinity anomaly. This could be associated to the absence of large freshwater volumes concentrated in that location as in the other years, or the footprint of larger AW inflows in summer/autumn from the WSC to the area north of Svalbard and the Western Nansen Basin (Duarte et al., 2020), which could intensify sea-ice melting.

Another important mechanism which could drive the inter-annual variability in winter density on the WSS and adjacent fjords may be related to the occurrence of extensive AW advection in the previous summer/autumn. As the case of summer/autumn 2016 featuring one of the strongest AW intrusions in Kongsfjorden of the decade (De Rovere et al., 2022), these events may leave a denser water column at the end of the year. Then, the freshwater carried by the SPC in the following months could not be enough by itself to significantly lower the density in the fjord, leaving the geostrophic control at the fjord mouth unaffected.

3.3 Downwelling event: 2014

The AW intrusion event in 2014 shows a different dynamic compared to the other years, i.e., through downwelling. Figure 8 reports the main oceanic and atmospheric physical parameters describing the event.

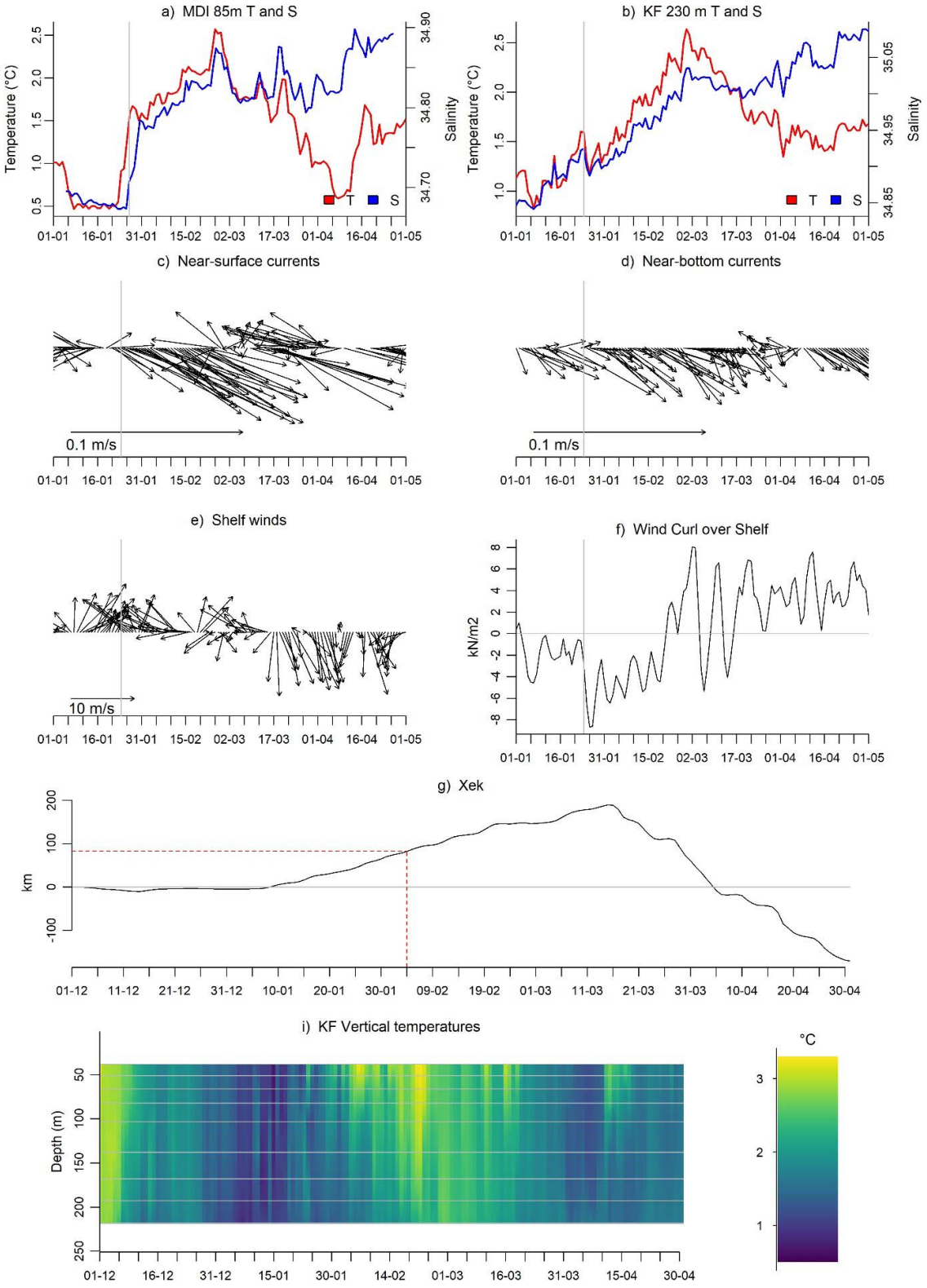

Figure 8: Winter 2014 AW intrusion: a) temperature and salinity at MDI; b) temperature and salinity at KF; c) near-surface currents from KF; d) near-bottom currents from KF; e) average winds over the shelf (area A1) from ERA5 ; f) average wind curl over the shelf (area A1) from

ERA5; g) cumulative net onshore displacement (X_{Ek}) calculated using average winds in A1 (see appendix C); i) KF temperature profile, gray horizontal lines identify sensors' depths.

In the downwelling event, warming starts from above and slowly reaches the near-bottom (Figure 8i). Near-bottom sensors at KF experienced a gradual warming and salinification from January to March (Figure 8b), while at mid-depth MDI detected a sudden increase in temperature and salinity (Figure 8a). Currents show inflowing velocities and higher values are seen in the near-surface (Figure 8c) compared to the near-bottom (Figure 8d). Shelf winds have blown almost constantly from the south from the end of January to the end of February (Figure 8e), instaurating downwelling conditions (Figure 8f). Winds in the fjord blew constantly from the south, bringing warm and humid air in Kongsfjorden (not shown). A peculiar difference with the previously described upwelling mechanism is the absence of wind *reversals* in this winter (Figure 4). We hypothesize that long-lasting, constant southerly winds transported the shallowest WSC layers toward the fjord, which were eventually forced to enter on top of fjord waters. The cumulative net onshore displacement ($X_{Ek,}$ see appendix C) shows that the theoretical Ekman layer covers the total distance between the shelf break (F3 location), where the WSC flows, and Kongsfjorden (KF location) in 64 days, thus arriving in the fjord at the beginning of February 2014 (see red dashed lines in Figure 8g). This result is in line with the first arrival of warm waters at the near-surface in KF in the same days (Figure 8i). Another critical point in this winter are the properties and the vertical extension of the WSC at the shelf break. 2014 is the second warmest winter at 70 m depth as well as the winter with the highest temperature difference between 70 and 250 m depth, according to 13 years of F3 measurements from 1999 to 2015 (Figure S7). This indicate that the core of the WSC is shallower in winter 2014 compared to the other years, and warm waters could have been more easily transported toward the coast of Spitsbergen. Figure 9 illustrates the specific atmospheric conditions of winter 2014.

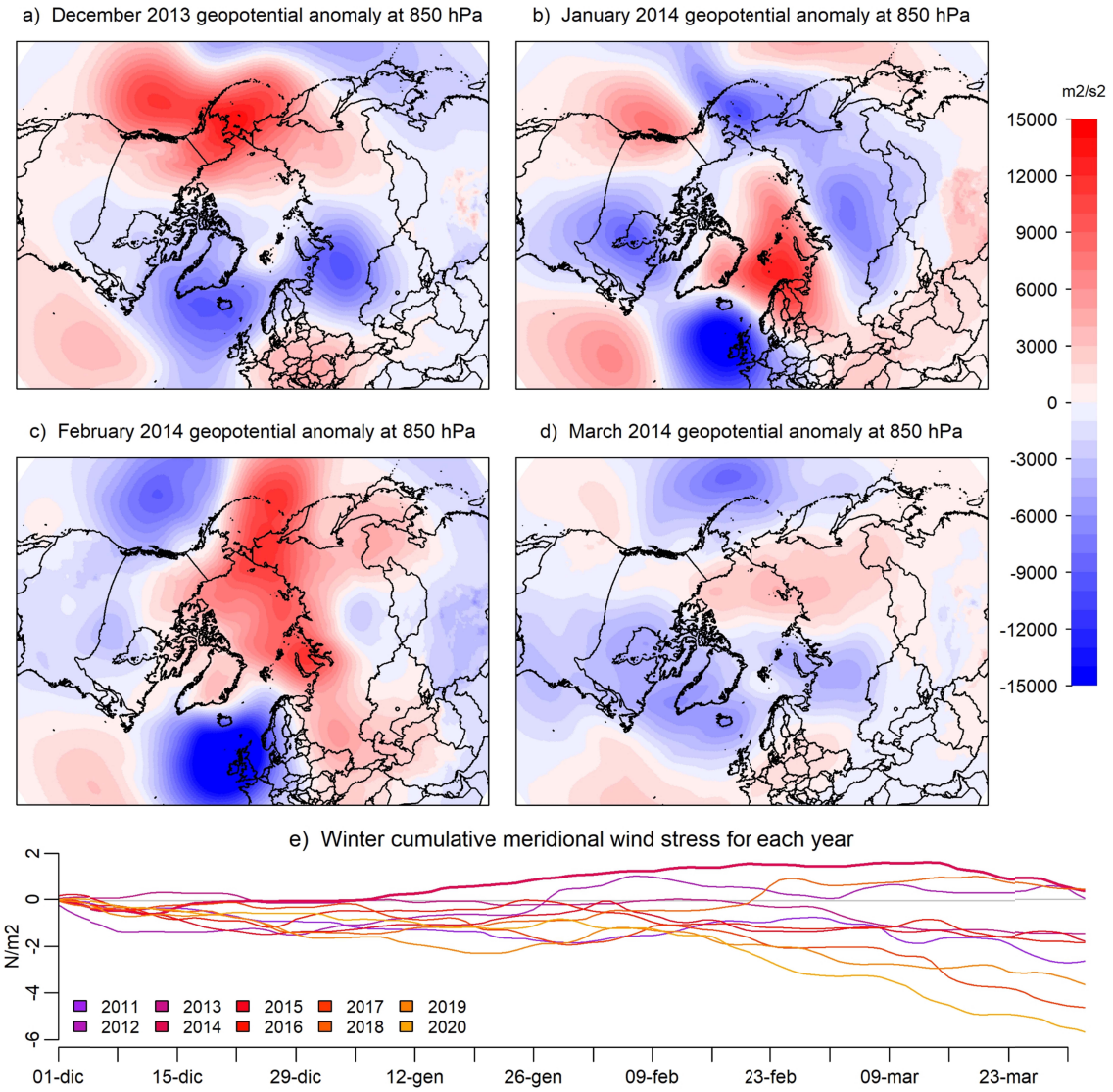

Figure 9: Atmospheric conditions in winter 2014. Mean geopotential anomaly at 850 hPa in December 2013 (a), January 2014 (b), February 2014 (c) and March 2014 (d). Climatology is computed over the 2011-2020 decade. (e) Cumulative meridional wind stress from December to April for winters in the 2011-2020 decade.

A strong positive geopotential anomaly centered in the Barents Sea develops in January 2014 (Figure 9b) and persists in February 2014 (Figure 9c), while a strong negative geopotential anomaly develops in the north-eastern Atlantic region, between Iceland and Great Britain. This particular atmospheric setting is similar to the one observed for upwelling events (Figure 4d), with an important difference. Indeed, this persistent positive geopotential anomaly generates southerly winds over the Fram Strait almost continuously for two months, as also reported by Figure 9e. Here, winter 2014 (thicker purple line) has a continuous

517 positive meridional wind stress, reaching the highest positive cumulative values of the
518 decade.

4. Summary and Conclusions

This paper examines the mechanisms of AW winter intrusions in Kongsfjorden through continuous mooring observations as well as atmospheric and oceanic reanalysis products. AW winter intrusions in the 2011-2020 decade are relatively common events, leading to a temperature and density increase of at least 1°C and 0.03 kg/m^3, respectively, in just a few days, and leaving a warmer and denser water column for a few weeks. Five events took place in winters 2011, 2012, 2016, 2018 and 2020 by means of upwelling. Intrusions are activated by energetic wind *reversal* events blowing over the WSS, causing strong southerly winds and downwelling conditions, followed by northerly winds and upwelling conditions. According to Nilsen et al. (2016), *reversals* move WSC waters on the shallower isobaths on the WSS, setting up the STC transporting AW toward Kongsfjorden. Southerlies are developed by the setup of a strong pressure dipole, with a high pressure center over the Barents Sea and a low pressure center over Greenland and Northern Canada. Afterwards, northerly winds are generated by the restoration of the normal low pressure conditions over the Central Arctic and the Svalbard archipelago. The occurrence of winter *reversal* events is significantly correlated to the mean winter AO conditions. Accordingly, the large meanders in the jet stream associated with the negative AO phase are more likely to trigger the geopotential dipole associated with atmospheric *reversals. Reversals* occurred almost every winter in the 2011-2020 decade, and thus are not the only key aspect driving AW intrusions. The ocean is a crucial preconditioning factor, limiting intrusions only to those winters characterized by a negative on-shore density gradient, i.e., when fjord waters are less dense than WSC waters, which disrupts the geostrophic control mechanism (Cottier et al., 2005). That is the case of all winters with AW intrusions by upwelling, where low density bottom waters in the fjord are linked to the external advection of fresher (2011, 2012, 2018, 2020) or warmer (2016) waters before the *onset* of the intrusion. We identified the SPC as the key driver of the freshwater input, which transport anomalously low salinity waters from the northern Barents Sea to the WSS, produced by the melting of large Arctic sea-ice volumes in the previous summer. We foreseen the Arctic sea-ice melting cycle to drive the variability in the SPC properties, which eventually freshens the WSS in some winters and allow the development of AW intrusions by upwelling. Instead, the warmer conditions seen in 2016 are the footprint of an extensive AW intrusion occurred in the second half of 2015. Winter 2014 AW intrusion occurred by means of downwelling, driven by the particular atmospheric pattern and oceanic conditions characterizing this winter. On the WSS, southerly winds have blown almost continuously during January and February, transporting waters from the top layers of the WSC toward Kongsfjorden. AW then intruded on top of fjord waters. Southerly winds have been induced by the set up of a long-lasting high pressure anomaly over the

555 Barents Sea and the Eurasian Arctic region, which contrasted a low pressure anomaly over
556 the north-eastern Atlantic Ocean.
557 The different AW intrusion mechanisms examined in this study relates to the winter
558 scenarios proposed by Tverberg et al. (2019), which link the character of the winter AW
559 intrusion in Kongsfjorden to the water column's structure in the following summer. The
560 upwelling mechanism is consistent with the *Winter Intermediate* scenario, where the AW
561 intrusion occurs at depth and, depending on the magnitude of the upwelling, it can reach the
562 fjord surface. Differently, the downwelling mechanism is consistent with the *Winter Open*
563 scenario, where the AW intrudes on top of fjord waters and spreads toward the bottom, likely
564 by cooling and densification. Finally, those winters characterized by the absence of an AW
565 intrusion are consistent with the *Winter Deep* scenario, where the fjord's water column
566 undergoes convection and densification, closing the fjord to the AW. Here, the larger fjord
567 densities are also benefiting from the extensive AW intrusion occurring in the previous
568 autumn season, leaving a saltier water column.
569 This study improved the understanding of winter AW intrusion mechanics by discussing the
570 dynamical aspects of two types of AW intrusion events. The emerging picture shows that
571 both the atmospheric and oceanic components are relevant in determining the timing and
572 inter-annual variability of upwelling events and, more generally, of Kongsfjorden's winter
573 conditions. Indeed, winters characterized by a negative AO phase and following a summer
574 with intense sea-ice melting have a very high chance to see the occurrence of an AW
575 intrusion. Furthermore, the SPC is revealed to play a critical role by transmitting the low
576 density signal from the northern Barents Sea over the WSS to the adjacent fjords. Given the
577 uttermost importance of the SPC for AW intrusions in Kongsfjorden, future studies should
578 focus on describing its seasonal and interannual variability, as well as identify the most
579 important factors regulating its properties.

Acknowledgements

ADCP and CTD data for mooring KF were provided by the Kongsfjorden Rijpfjorden Observatory Program (KROP) which has been supported by the UK Natural Environment Research Council (Oceans 2025 and Northern Sea Program) and the Research Council of Norway (projects Cleopatra: 178766, Cleopatra II: 216537, Circa: 214271/ F20, Marine Night: 26471, FAABulous: 243702, ArcticABC: 244319 and Deep Impact: 300333). We would like to acknowledge the UNIS courses AB-320 and AB-321 for the cooperation in the use of ship time.

We thank Daniel Ludwig Vogedes for sharing the ADCP data for KF.

Open research

MDI and CCT data (CNR – National Research Council of Italy, 2022) can be found in the Italian Arctic Data Center at https://data.iadc.cnr.it/erddap/files/mdi_ctd_timeseries_1/.

KF temperature and salinity data (Cottier et al., 2021a, 2021b, 2021c; Cottier et al., 2022a, 2022b, 2022,c, 2022d, 2022e, 2022f, 2022g, 2022h, 2022i) can be found in the NIRD research data archive (archive.sigma2.no/). KF raw ADCP data can be requested to daniel.vogedes@uit.no and will be updated in the NIRD research data archive.

F3 data (Beszczynska-Möller et al., 2012a, 2015; von Appen et al., 2015, 2017) can be found in the PANGAEA data archive (doi.pangaea.de/10.1594/PANGAEA.900883).

I1 data (Skogseth and Ellingsen, 2019a, 2019b, 2019c, 2019d, 2019e, 2019f, 2019g, 2019h) can be found at the Norwegian Polar Data Centre (data.npolar.no/home/).

ERA5 data (Hersbach et al., 2023a, 2023b) are available from the Copernicus program at doi.org/10.24381/cds.adbb2d47 for hourly data on single levels and at doi.org/10.24381/cds.bd0915c6 for hourly data on pressure levels.

CMEMS Arctic Ocean Physics Reanalysis data (CMEMS – Copernicus Marine Service, 2022) are available from the E.U. Copernicus Marine Service Information at doi.org/10.48670/moi-00007.

Appendixes

Appendix A: Significance analysis for Figure 4d and 4e

Figure 4d,e are an average of the geopotential anomalies observed in the week before and after the onset of *reversals* occurred in winters over the 2011-2020 decade, for a total of 18 events. We assess the significance of these mean anomalies as follows: 18 casual dates over 2011-2020 winters are selected as *onsets*. The associated mean geopotential anomalies of the week before and after these 18 casual dates are calculated. We repeat this step 100 times to produce a distribution of geopotential mean anomalies observed in the week before and after casual dates. In Figure 4d,e, gray crosses identify locations with non-significant geopotential anomalies, i.e., with a mean geopotential anomaly calculated over the 18 selected *reversals* falling within the 10^{th}-90^{th} percentiles interval of the casual distribution of geopotential mean anomalies. Those locations without gray crosses feature locations with significant geopotential anomalies, i.e., with a mean geopotential which is either <10th or >90th percentile of the casual distribution of geopotential mean anomalies.

Appendix B: Significance analysis of Figure 7

Figure 7 reports the difference between the averages of two pools of salinity fields from the CMEMS Arctic Ocean Reanalysis. The statistical significance of this difference is examined at each location by performing a non-parametric test (Mann-Whitney-Wilcoxon) on the two pools defining the two averages, to verify if they come from the same distribution at the 99% confidence level. Locations whose differences are associated to non-significantly different pools are marked in gray.

Appendix C: Calculation of the Cumulative Net Onshore Displacement (X_{Ek}) reported in Figure 8

X_{Ek} is calculated using the following formula, from Cushman-Roisin and Beckers (2011):

$$X_{Ek} = \frac{I}{f}$$

where *f* is the coriolis parameter and *I* is the *wind impulse*, represented as:

$$I \simeq \frac{1}{\rho_0 H} \int_{event} \tau_y \, dt$$

where ρ_0 is the initial density (here set to 1027.85 Kg/m3), *H* the depth of the Ekman layer and τ_y the daily meridional wind stress average over A1 (from ERA5 data). *H* is estimated as the theoretical Ekman layer depth:

$$H = \sqrt{2K_m/|f|}$$

where K_m is the turbulent diffusivity, assumed to be 0.1 m^2/s and f the Coriolis parameter. At 78.8 °N, d_{Ek} is equal to 11.8 m.

642 **Authors contributions statement**

643 FDR evolved the initial idea and together with DZ and JC developed the study. AR helped in
644 the interpretation of the dynamics. FC first approached this thematic in his master thesis,
645 under the supervision of FDR, PR, AL and LL. AL provided the *in-situ* atmospheric data from
646 the CCT, while LL provided the marine data from MDI. All analyses were performed by FDR,
647 except for Figure 1, based on the master thesis work of FC. FDR wrote the manuscript with
648 inputs from all authors.

649 **References**
650
651 1. Beszczynska-Möller, Agnieszka, Fahrbach, Eberhard. Rohardt, Gerd, Schauer,
652 Ursula (2012a). Physical oceanography and current meter data from mooring F3-13
653 [Dataset]. PANGAEA. https://doi.org/10.1594/PANGAEA.800342
654
655 2. Beszczynska-Möller, A., Fahrbach, E., Schauer, U., & Hansen, E. (2012b). Variability
656 in Atlantic water temperature and transport at the entrance to the Arctic Ocean,
657 1997–2010. *ICES Journal of Marine Science*, *69*(5), 852-863.
658
659 3. Beszczynska-Möller, Agnieszka, von Appen, Wilken-Jon, Fahrbach, Eberhard
660 (2015). Physical oceanography and current meter data from mooring F3-14
661 [Dataset]. PANGAEA. https://doi.org/10.1594/PANGAEA.845648
662
663 4. Bloshkina, E. V., Pavlov, A. K., & Filchuk, K. (2021). Warming of Atlantic Water in
664 three west Spitsbergen fjords: recent patterns and century-long trends. Polar
665 Research, 40.
666
667 5. Carmack, E., Polyakov, I., Padman, L., Fer, I., Hunke, E., Hutchings, J., ... & Winsor,
668 P. (2015). Toward quantifying the increasing role of oceanic heat in sea ice loss in
669 the new Arctic. Bulletin of the American Meteorological Society, 96(12), 2079-2105.
670
671 6. Chatterjee, S., Raj, R. P., Bertino, L., Skagseth, Ø., Ravichandran, M., &
672 Johannessen, O. M. (2018). Role of Greenland Sea gyre circulation on Atlantic water
673 temperature variability in the Fram Strait. Geophysical Research Letters, 45(16),
674 8399-8406.
675
676 7. Chree, C., (1912). Some phenomena of sunspots and of terrestrial magnetism, at
677 Kew observatory. Philosophical Transactions Royal Society London Series A 212,
678 75.
679
680 8. Chree, C., (1913). Some phenomena of sunspots and of terrestrial magnetism, II.
681 Philosophical Transactions Royal Society London Series A 213, 245.
682
683 9. Chylek, P., Folland, C. K., Lesins, G., Dubey, M. K., & Wang, M. (2009). Arctic air
684 temperature change amplification and the Atlantic Multidecadal Oscillation.
685 Geophysical Research Letters, 36(14).

10. CNR – National Research Council of Italy (2022). CTD data set from mooring MDI @ 35m and 85m (Kongsfjorden) [Dataset]. Italian Arctic Data Center. https://data.iadc.cnr.it/erddap/info/mdi_ctd_timeseries_1/index.html.

11. Comiso, J. C. (2012). Large decadal decline of the Arctic multiyear ice cover. Journal of climate, 25(4), 1176-1193.

12. CMEMS - Copernicus Marine Service (2022). Arctic Ocean Physics Reanalysis [Dataset]. Copernicus Marine Data Store. https://doi.org/10.48670/moi-00007.

13. Cottier, F., Tverberg, V., Inall, M., Svendsen, H., Nilsen, F., & Griffiths, C. (2005). Water mass modification in an Arctic fjord through cross□shelf exchange: The seasonal hydrography of Kongsfjorden, Svalbard. *Journal of Geophysical Research: Oceans*, *110*(C12).

14. Cottier, F. R., Nilsen, F., Inall, M. E., Gerland, S., Tverberg, V., & Svendsen, H. (2007). Wintertime warming of an Arctic shelf in response to large□scale atmospheric circulation. *Geophysical Research Letters*, *34*(10).

15. Cottier, F., Skogseth, R., David, D., and Berge, J. (2019). “Temperature time-series in Svalbard fjords. A contribution from the “Integrated Marine Observatory Partnership(iMOP)”,” in The e State of Environmental Science in Svalbard report 2018, eds E. Orr, G. Hansen, H. Lappalainen, C. Hübner, and H. Lihavainen (Longyearbyen: Svalbard Integrated Arctic Earth Observing System), 108–118.

16. Cottier, F., Berge, J., Griffith, C., Dumont, E., Beaton, J., Vogedes, D. L., UiT The Arctic University of Norway, Scottish Association for Marine Science (2021a). Temperature, salinity, light and fluorescence (CTD) measurements from the Kongsfjorden (Svalbard) marine observatory (mooring) September 2015-August 2016 [Dataset]. Norstore. https://doi.org/10.11582/2021.00061

17. Cottier, F., Berge, J., Dumont, E., Griffith, C., Beaton, J., Vogedes, D. L., UiT The Arctic University of Norway, Scottish Association for Marine Science (2021b). Temperature, salinity, light and fluorescence (CTD) measurements from the Kongsfjorden (Svalbard) marine observatory (mooring) August 2016-August 2017 [Dataset]. Norstore. https://doi.org/10.11582/2021.00062

18. Cottier, F., Berge, J., Dumont, E., Kopec, T. P., Venables, E. J., Vogedes, D. L., UiT The Arctic University of Norway, Scottish Association for Marine Science (2021c). Temperature, salinity, light and fluorescence (CTD) measurements from the Kongsfjorden (Svalbard) marine observatory (mooring) August 2017-August 2018 [Dataset]. Norstore. https://doi.org/10.11582/2021.00065

19. Cottier, F., Berge, J., Griffith, C., Dumont, E., Kopec, T. P., Vogedes, D. L., UiT The Arctic University of Norway, Scottish Association for Marine Science (2022a). Temperature, salinity and fluorescence (CTD) measurements from the Kongsfjorden (Svalbard) marine observatory (mooring) June 2006-August 2007 [Dataset]. Norstore. https://doi.org/10.11582/2022.00024

20. Cottier, F., Berge, J., Griffith, C., Dumont, E., Kopec, T. P., Vogedes, D. L., UiT The Arctic University of Norway, Scottish Association for Marine Science (2022b). Temperature, salinity, light and fluorescence (CTD) measurements from the Kongsfjorden (Svalbard) marine observatory (mooring) August 2007-August 2008 [Dataset]. Norstore. https://doi.org/10.11582/2022.00025

21. Cottier, F., Berge, J., Griffith, C., Dumont, E., Kopec, T. P., Vogedes, D. L., UiT The Arctic University of Norway, Scottish Association for Marine Science (2022c). Temperature, salinity, light and fluorescence (CTD) measurements from the Kongsfjorden (Svalbard) marine observatory (mooring) September 2008-August 2009 [Dataset]. Norstore. https://doi.org/10.11582/2022.00026

22. Cottier, F., Berge, J., Griffith, C., Dumont, E., Kopec, T. P., Vogedes, D. L., UiT The Arctic University of Norway, Scottish Association for Marine Science (2022d). Temperature, salinity, light and fluorescence (CTD) measurements from the Kongsfjorden (Svalbard) marine observatory (mooring) September 2009-September 2010 [Dataset]. Norstore. https://doi.org/10.11582/2022.00022

23. Cottier, F., Griffith, C., Dumont, E., Kopec, T. P., Vogedes, D. L., UiT The Arctic University of Norway, Scottish Association for Marine Science (2022e). Temperature, salinity, light and fluorescence (CTD) measurements from the Kongsfjorden (Svalbard) marine observatory (mooring) September 2010-September 2011 [Dataset]. Norstore. https://doi.org/10.11582/2022.00023

24. Cottier, F., Berge, J., Griffith, C., Dumont, E., Kopec, T. P., Vogedes, D. L. (2022f). Temperature, salinity, light and fluorescence (CTD) measurements from the Kongsfjorden (Svalbard) marine observatory (mooring) September 2011-September 2012 [Dataset]. Norstore. https://doi.org/10.11582/2022.00020

25. Cottier, F., Berge, J., Griffith, C., Dumont, E., Kopec, T. P., Vogedes, D. L., UiT The Arctic University of Norway, Scottish Association for Marine Science (2022g). Temperature, salinity, light and fluorescence (CTD) measurements from the Kongsfjorden (Svalbard) marine observatory (mooring) October 2012-September 2013 [Dataset]. Norstore. https://doi.org/10.11582/2022.00021

26. Cottier, F., Berge, J., Griffith, C., Dumont, E., Beaton, J., Vogedes, D. L., UiT The Arctic University of Norway, Scottish Association for Marine Science (2022h). Temperature, salinity, light and fluorescence (CTD) measurements from the Kongsfjorden (Svalbard) marine observatory (mooring) September 2013-October 2014 [Dataset]. Norstore. https://doi.org/10.11582/2022.00018

27. Cottier, F., Berge, J., Griffith, C., Dumont, E., Beaton, J., Vogedes, D. L., Kopec, T. P., UiT The Arctic University of Norway, Scottish Association for Marine Science (2022i).Temperature, salinity, light and fluorescence (CTD) measurements from the Kongsfjorden (Svalbard) marine observatory (mooring) September 2014-September 2015 [Dataset]. Norstore. https://doi.org/10.11582/2022.00019

28. Curry, J. A., Schramm, J. L., & Ebert, E. E. (1995). Sea ice-albedo climate feedback mechanism. Journal of Climate, 8(2), 240-247.

29. Cushman-Roisin, B., & Beckers, J. M. (2011). Introduction to geophysical fluid dynamics: physical and numerical aspects. Academic press.

30. D'Angelo, A., Giglio, F., Miserocchi, S., Sanchez-Vidal, A., Aliani, S., Tesi, T., et al. (2018). Multi-year particle fluxes in Kongsfjorden, Svalbard. Biogeosciences 15, 5343–5363

31. De Rovere, F., Langone, L., Schroeder, K., Miserocchi, S., Giglio, F., Aliani, S., & Chiggiato, J. (2022). Water Masses Variability in Inner Kongsfjorden (Svalbard) During 2010–2020. Frontiers in Marine Science, 9.

32. Duarte, P., Sundfjord, A., Meyer, A., Hudson, S. R., Spreen, G., & Smedsrud, L. H. (2020). Warm Atlantic water explains observed sea ice melt rates north of Svalbard. Journal of Geophysical Research: Oceans, 125(8), e2019JC015662.

33. Häkkinen, S., Rhines, P. B., & Worthen, D. L. (2011). Atmospheric blocking and Atlantic multidecadal ocean variability. Science, 334(6056), 655-659.

34. Hegseth, E. N., & Tverberg, V. (2013). Effect of Atlantic water inflow on timing of the phytoplankton spring bloom in a high Arctic fjord (Kongsfjorden, Svalbard). Journal of Marine Systems, 113, 94-105.

35. Helland□Hansen, B., & Nansen, F. (1909). Die jährlichen Schwankungen der Wassermassen im norwegischen Nordmeer in ihrer Beziehung zu den Schwankungen der meteorologischen Verhältnisse, der Ernteerträge und der Fischereiergebnisse in Norwegen. Internationale Revue der gesamten Hydrobiologie und Hydrographie, 2(3), 337-361.

36. Hersbach, H., Bell, B., Berrisford, P., Biavati, G., Horányi, A., Muñoz Sabater, J., Nicolas, J., Peubey, C., Radu, R., Rozum, I., Schepers, D., Simmons, A., Soci, C., Dee, D., Thépaut, J-N. (2023a): ERA5 hourly data on pressure levels from 1940 to present. Copernicus Climate Change Service (C3S) Climate Data Store (CDS), DOI: 10.24381/cds.bd0915c6

37. Hersbach, H., Bell, B., Berrisford, P., Biavati, G., Horányi, A., Muñoz Sabater, J., Nicolas, J., Peubey, C., Radu, R., Rozum, I., Schepers, D., Simmons, A., Soci, C., Dee, D., Thépaut, J-N. (2023b): ERA5 hourly data on single levels from 1940 to present. Copernicus Climate Change Service (C3S) Climate Data Store (CDS), DOI: 10.24381/cds.adbb2d47

38. Holmes, F. A., Kirchner, N., Kuttenkeuler, J., Krützfeldt, J., & Noormets, R. (2019). Relating ocean temperatures to frontal ablation rates at Svalbard tidewater glaciers: Insights from glacier proximal datasets. Scientific reports, 9(1), 1-11.

39. Hop, H., & Wiencke, C. (2019). The Ecosystem of Kongsfjorden, Svalbard (pp. 1-20). Springer International Publishing.

40. Inall, M. E., Nilsen, F., Cottier, F. R., & Daae, R. (2015). Shelf/fjord exchange driven by coastal□trapped waves in the Arctic. Journal of Geophysical Research: Oceans, 120(12), 8283-8303.

41. Ingvaldsen, R. B., Assmann, K. M., Primicerio, R., Fossheim, M., Polyakov, I. V., & Dolgov, A. V. (2021). Physical manifestations and ecological implications of Arctic Atlantification. Nature Reviews Earth & Environment, 2(12), 874-889.

42. Jackson, R. H., Straneo, F., & Sutherland, D. A. (2014). Externally forced fluctuations in ocean temperature at Greenland glaciers in non-summer months. Nature Geoscience, 7(7), 503-508.

43. Klinck, J. M., O'Brien, J. J., & Svendsen, H. (1981). A simple model of fjord and coastal circulation interaction. *Journal of Physical Oceanography*, *11*(12), 1612-1626.

44. Lind, S., Ingvaldsen, R. B., & Furevik, T. (2018). Arctic warming hotspot in the northern Barents Sea linked to declining sea-ice import. Nature climate change, 8(7), 634-639.

45. Luckman, A., Benn, D. I., Cottier, F., Bevan, S., Nilsen, F., & Inall, M. (2015). Calving rates at tidewater glaciers vary strongly with ocean temperature. Nature communications, 6(1), 1-7.

46. Lundesgaard, Ø., Sundfjord, A., Lind, S., Nilsen, F., & Renner, A. H. (2022). Import of Atlantic Water and sea ice controls the ocean environment in the northern Barents Sea. Ocean Science, 18(5), 1389-1418.

47. Meredith, M., M. Sommerkorn, S. Cassotta, C. Derksen, A. Ekaykin, A. Hollowed, G. Kofinas, A. Mackintosh, J. Melbourne-Thomas, M.M.C. Muelbert, G. Ottersen, H. Pritchard, and E.A.G. Schuur, 2019: Polar Regions. In: IPCC Special Report on the Ocean and Cryosphere in a Changing Climate [H.-O. Pörtner, D.C. Roberts, V. Masson-Delmotte, P. Zhai, M. Tignor, E. Poloczanska, K. Mintenbeck, A. Alegría, M. Nicolai, A. Okem, J. Petzold, B. Rama, N.M. Weyer (eds.)]. Cambridge University Press, Cambridge, UK and New York, NY, USA, pp. 203–320. https://doi.org/10.1017/9781009157964.005.

869 48. Muilwijk, M., Smedsrud, L. H., Ilicak, M., & Drange, H. (2018). Atlantic Water heat
870 transport variability in the 20th century Arctic Ocean from a global ocean model and
871 observations. Journal of Geophysical Research: Oceans, 123(11), 8159-8179.
872
873 49. Nilsen, F., Gjevik, B., & Schauer, U. (2006). Cooling of the West Spitsbergen
874 Current: Isopycnal diffusion by topographic vorticity waves. Journal of Geophysical
875 Research: Oceans, 111(C8).
876
877 50. Nilsen, F., Skogseth, R., Vaardal-Lunde, J., & Inall, M. (2016). A simple shelf
878 circulation model: intrusion of Atlantic Water on the West Spitsbergen Shelf. *Journal*
879 *of Physical Oceanography*, *46*(4), 1209-1230.
880
881 51. Payne, C. M., & Roesler, C. S. (2019). Characterizing the influence of Atlantic water
882 intrusion on water mass formation and phytoplankton distribution in Kongsfjorden,
883 Svalbard. Continental Shelf Research, 191, 104005.
884
885 52. Polyakov, I. V., Pnyushkov, A. V., Alkire, M. B., Ashik, I. M., Baumann, T. M.,
886 Carmack, E. C., ... & Yulin, A. (2017). Greater role for Atlantic inflows on sea-ice loss
887 in the Eurasian Basin of the Arctic Ocean. *Science*, *356*(6335), 285-291.
888
889 53. Raj, R. P., Nilsen, J. Ø., Johannessen, J. A., Furevik, T., Andersen, O. B., & Bertino,
890 L. (2018). Quantifying Atlantic Water transport to the Nordic Seas by remote sensing.
891 Remote Sensing of Environment, 216, 758-769.
892
893 54. Richter-Menge, J., & Druckenmiller, M. L. (2020). State of the climate in 2019. Arctic,
894 101(8), S239-S286.
895
896 55. Rogers, J. C., Yang, L., & Li, L. (2005). The role of Fram Strait winter cyclones on
897 sea ice flux and on Spitsbergen air temperatures. Geophysical Research Letters,
898 32(6).
899
900 56. Ruggieri, P., Alvarez-Castro, M. C., Athanasiadis, P., Bellucci, A., Materia, S., &
901 Gualdi, S. (2020). North Atlantic circulation regimes and heat transport by synoptic
902 eddies. Journal of Climate, 33(11), 4769-4785.
903
904 57. Serreze, M. C., & Barry, R. G. (2011). Processes and impacts of Arctic amplification:
905 A research synthesis. Global and planetary change, 77(1-2), 85-96.

58. Singh, Y. P. (2006). Statistical considerations in superposed epoch analysis and its applications in space research. Journal of atmospheric and solar-terrestrial physics, 68(7), 803-813.

59. Skogseth, R., & Ellingsen, P. G. (2019a). Mooring data from the Isfjorden Mouth - South (I-S) during 9 Sep 2010 to 3 Sep 2011 [Dataset]. Norwegian Polar Institute. https://doi.org/10.21334/npolar.2019.b0e473c4

60. Skogseth, R., & Ellingsen, P. G. (2019b). Mooring data from the Isfjorden Mouth - South (I-S) during 8 Sep 2011 to 3 Sep 2012 [Dataset]. Norwegian Polar Institute. https://doi.org/10.21334/npolar.2019.2be7bdee

61. Skogseth, R., & Ellingsen, P. G. (2019c). Mooring data from the Isfjorden Mouth - South (I-S) during 6 Sep 2012 to 28 Aug 2013 [Dataset]. Norwegian Polar Institute. https://doi.org/10.21334/npolar.2019.a247e9a9

62. Skogseth, R., & Ellingsen, P. G. (2019d). Mooring data from the Isfjorden Mouth - South (I-S) during 2 Sep 2013 to 26 Aug 2014 [Dataset]. Norwegian Polar Institute. https://doi.org/10.21334/npolar.2019.6813ce6d

63. Skogseth, R., & Ellingsen, P. G. (2019e). Mooring data from the Isfjorden Mouth - South (I-S) during 31 Aug 2014 to 24 Aug 2015 [Dataset]. Norwegian Polar Institute. https://doi.org/10.21334/npolar.2019.11b7e849

64. Skogseth, R., & Ellingsen, P. G. (2019f). Mooring data from the Isfjorden Mouth - South (I-S) during 31 Aug 2015 to 12 Aug 2016 [Dataset]. Norwegian Polar Institute. https://doi.org/10.21334/npolar.2019.21838303

65. Skogseth, R., & Ellingsen, P. G. (2019g). Mooring data from the Isfjorden Mouth - South (I-S) during 19 Aug 2016 to 2 Oct 2017 [Dataset]. Norwegian Polar Institute. https://doi.org/10.21334/npolar.2019.cd7a2f7c

66. Skogseth, R., & Ellingsen, P. G. (2019h). Mooring data from the Isfjorden Mouth - South (I-S) during 5 Oct 2017 to 25 Aug 2018 [Dataset]. Norwegian Polar Institute. https://doi.org/10.21334/npolar.2019.54dcd0c9

943 67. Skogseth, R., Olivier, L. L., Nilsen, F., Falck, E., Fraser, N., Tverberg, V., ... & Falk-
944 Petersen, S. (2020). Variability and decadal trends in the Isfjorden (Svalbard) ocean
945 climate and circulation–An indicator for climate change in the European Arctic.
946 Progress in Oceanography, 187, 102394.
947
948 68. Stigebrandt, A. (1981). A mechanism governing the estuarine circulation in deep,
949 strongly stratified fjords. Estuarine, Coastal and Shelf Science, 13(2), 197-211.
950
951 69. Straneo, F., Hamilton, G. S., Sutherland, D. A., Stearns, L. A., Davidson, F., Hammill,
952 M. O., ... & Rosing-Asvid, A. (2010). Rapid circulation of warm subtropical waters in a
953 major glacial fjord in East Greenland. Nature Geoscience, 3(3), 182-186.
954
955 70. Strzelewicz, A., Przyborska, A., & Walczowski, W. (2022). Increased presence of
956 Atlantic Water on the shelf south-west of Spitsbergen with implications for the Arctic
957 fjord Hornsund. Progress in Oceanography, 200, 102714.
958
959 71. Svendsen, H. (1980). Exchange processes above sill level between fjords and
960 coastal water. In Fjord oceanography (pp. 355-361). Springer, Boston, MA.
961
962 72. Svendsen, H., Beszczynska-Møller, A., Hagen, J. O., Lefauconnier, B., Tverberg, V.,
963 Gerland, S., ... & Wiencke, C. (2002). The physical environment of Kongsfjorden–
964 Krossfjorden, an Arctic fjord system in Svalbard. Polar research, 21(1), 133-166.
965
966 73. Teigen, S. H., Nilsen, F., & Gjevik, B. (2010). Barotropic instability in the West
967 Spitsbergen Current. Journal of Geophysical Research: Oceans, 115(C7).
968
969 74. Teigen, S. H., Nilsen, F., Skogseth, R., Gjevik, B., & Beszczynska□Möller, A. (2011).
970 Baroclinic instability in the West Spitsbergen current. Journal of Geophysical
971 Research: Oceans, 116(C7).
972
973 75. Tverberg, V., Skogseth, R., Cottier, F., Sundfjord, A., Walczowski, W., Inall, M. E., ...
974 & Nilsen, F. (2019). The Kongsfjorden transect: seasonal and inter-annual variability
975 in hydrography. In *The Ecosystem of Kongsfjorden, Svalbard* (pp. 49-104). Springer,
976 Cham.
977
978 76. Vihtakari, M. (2020). PlotSvalbard: PlotSvalbard - Plot research data from Svalbard
979 on maps. R package version 0.9.2. https://github.com/MikkoVihtakari/PlotSvalbard

77. Vihtakari, M., Welcker, J., Moe, B., Chastel, O., Tartu, S., Hop, H., ... & Gabrielsen, G. W. (2018). Black-legged kittiwakes as messengers of Atlantification in the Arctic. Scientific Reports, 8(1), 1-11.

78. von Appen, Wilken-Jon; Beszczynska-Möller, Agnieszka; Fahrbach, Eberhard (2015): Physical oceanography and current meter data from mooring F3-15 [Dataset]. PANGAEA https://doi.org/10.1594/PANGAEA.853902

79. von Appen, Wilken-Jon; Latarius, Katrin; Kanzow, Torsten (2017): Physical oceanography and current meter data from mooring F3-16 [dataset]. PANGAEA. https://doi.org/10.1594/PANGAEA.870842

80. Walczowski, W., & Piechura, J. (2011). Influence of the West Spitsbergen Current on the local climate. International journal of climatology, 31(7), 1088-1093.

81. Wang, Q., Wekerle, C., Wang, X., Danilov, S., Koldunov, N., Sein, D., ... & Jung, T. (2020). Intensification of the Atlantic Water supply to the Arctic Ocean through Fram Strait induced by Arctic sea ice decline. Geophysical Research Letters, 47(3), e2019GL086682.

82. Zahn, M., Akperov, M., Rinke, A., Feser, F., & Mokhov, I. I. (2018). Trends of cyclone characteristics in the Arctic and their patterns from different reanalysis data. Journal of Geophysical Research: Atmospheres, 123(5), 2737-2751.